Acute Cannabidiol (CBD), Tetrahydrocannabinol (THC) and their mixture (THC:CBD) exert differential effects on brain activity and blood flow in rats: A Translational Neuroimaging Study

MacNicol et al.

Supplementary materials

Supplementary Methods

Vehicle preparation

Two separate vehicle formulations comprised of rats with “Vehicle 1” (5 % ethanol: 5 % Kolliphor EL in saline) (n = 6), and rats with “Vehicle 2” (10 % ethanol, 5 % Kolliphor EL in saline) (n = 5). Ethanol and Kolliphor EL were purchased from SigmaAldrich UK. Initial experiments tested for any statistical differences in brain activity between the two vehicles and found no significant differences in strength or diversity (not shown). Moreover, no differences survived FDR correction ($p > 0.05$) using the network-based statistics toolbox with an initial threshold of $t > 2.2$ (Cohen’s $d = (t)/\sqrt{n} = (2.2)/\sqrt{11} = 0.66$). Finally, there were also no significant differences in cerebral blood flow (CBF). Therefore, Vehicles 1 and 2 were combined into one group, hereafter referred to as “Vehicle” (n = 11 total number of animals in this group).

Experimental Design

Thirty minutes following drug administration, rats were anaesthetised with 5 % isoflurane in oxygen: air (10:90) for approximately 3 minutes after which isoflurane was lowered to 2.5 % and the rat was placed inside the scanner bed and the radiofrequency (RF) coil. After approximately 10 minutes, once positioned and attached to physiological monitoring equipment to measure temperature, respiration and heart rate (SA instruments Inc.), a bolus of medetomidine (medetomidine hydrochloride, ‘Dormitor’, Orion Pharma, 0.05 mg/kg, s.c. in 1µL/g volume) was given and the s.c. cannula attached to the infusion line. A timer was started at the administration of the bolus to provide consistent timings between animals and groups: isoflurane was reduced gradually to 0% over the first 10 minutes post-bolus and an infusion of 0.1 mg/kg/hr (in 2µL/g/hr) medetomidine was started at 15 minutes post-bolus. The timing of BOLD scans was adjusted to start approximately 105 (108±5.2) minutes from drug administration, with CBF scan starting approximately 15 minutes later.

Imaging Acquisition parameters

For structural (RARE) scan the parameters were: RARE factor = 10, Echo time (TE) = 44 ms, Repetition time (TR) = 5000 ms, 2 averages, Field of View (FOV) = 30 x 30 mm, matrix = 300 x 300, slice thickness = 0.6 mm, 46 contiguous slices, bandwidth = 100 kHz, scan time 5 min.

Rs fMRI data were acquired with a gradient-echo EPI using the following parameters: TE = 15 ms, TR = 1500 ms, 600 repetitions, FOV = 24 x 19.2 mm, matrix = 60 x 48, partial-FT acceleration factor = 1.2 in phase-encoding direction, slice thickness = 0.6 mm, 36 contiguous slices, bandwidth = 300 kHz, scan time 15 min.

Continuous arterial spin labelling (CASL) data were acquired using a spin-echo EPI sequence with parameters: TE = 14.1 ms, TR = 4000 ms, 60 control/label image pairs, labelling time = 3000 ms, post-labelling delay = 300 ms, FOV = 25 x 25 mm, matrix = 100 x 100, partial-FT acceleration factor = 1.69 in phase-encoding direction, slice thickness = 1 mm, slice gap = 0.2 mm, 18 slices, bandwidth = 375 kHz, scan time 8 min.

CBF pre-processing

Arterial spin labelling images were first motion corrected using AFNI's 3dvolreg (https://afni.nimh.nih.gov) and then distortion corrected using FSL's top up (Andersson et al., 2003). ANTs' N4BiasFieldCorrection (Tustison et al., 2010) was used to create an intensity bias corrected image of the mean of the ASL timeseries, which was used to derive a brain mask with RATS (Oguz et al., 2014). The motion and distortion corrected timeseries were then registered to the structural image using antsRegistration (ANTs; (Klein et al., 2009))and the inverse transforms, calculated between the structural and a rat brain template (Valdes Hernandez et al., 2021), applied to the corrected ASL time series resulting in images spatially registered to the template's space. Finally, cerebral blood flow maps were calculated (in ml/100 g/min) using QUantitative Imaging Tools (QUIT) software (Wood, 2016).

BOLD pre-processing

Resting state functional images were slice time corrected using AFNI's 3dTshift, motion corrected using AFNI's 3dvolreg and then distortion corrected using FSL's topup. The motion and distortion corrected timeseries was corrected for non-uniform intensity bias (ANTs' N4BiasFieldCorrection) and the temporal mean across the bias-corrected time series was calculated to derive a brain mask with RATS. The motion corrected timeseries were then registered to the structural image using antsRegistration (ANTs) and the inverse transforms calculate between the structural and a rat brain template (Valdes Hernandez et al., 2013) applied to the corrected resting state time series, resulting in images spatially normalised to the template's space. Timeseries were then spatially smoothed using a FWHM of 1 mm

(3dBlurInMask – AFNI). Motion correction parameters, mean CSF signal and mean vascular signal were regressed out of the functional time series using 3dTproject (AFNI), which employed a simultaneous band-pass filter between 0.01 and 0.1 Hz (Hallquist et al., 2013).

Voxelwise comparisons (BOLD and CBF)

An in-house Matlab® application was used to calculate the mean signal time course from 152 regions of interest (Kim et al., 2023) (ROIs; Supplementary Figure 2A) for each of the subject's pre-processed resting state data. Pearson's Correlation Coefficient (r) was then calculated between the signal in each ROI and all other voxels (ROI to Voxel) (Liang et al., 2013), resulting in 3D correlation maps for the whole brain. Fisher z-transform was also calculated for each 3D correlation map (according to the formula z=arctanh(r)).

For the BOLD data, group differences in Fisher transformed maps were calculated for the 14 bilateral *a priori* selected ROIs (Supplementary Figure 2B). In comparison, group differences in mean CBF values were calculated.

Group differences were estimated using a two-sample t-test (SPM12, https://www.fil.ion.ucl.ac.uk/spm/software/spm12/). The two-tailed contrast between the drug and vehicle was enhanced using the SPM probabilistic Threshold-Free Cluster Enhancement (pTFCE) toolbox (Spisak et al., 2019), which provided voxelwise p-value maps for the contrast. The results are demonstrated using the dual-coding approach (Sadagopan et al., 2015; van Lieshout et al., 2018; Batalla et al., 2014): the effect size, i.e., the magnitude of the difference between drug – vehicle, is represented by the colour of the overlay. Reds indicate areas where correlation with the seed timecourse or blood flow, respectively, is significantly higher in the drug treated group compared to vehicle; blue indicates areas the converse. The overlay opacity increases with the 1-p value derived from the statistical parametric maps. Additionally, regional contours denote voxels that surpass a significance threshold of $p < 0.001$ uncorrected for the two-tailed, two-sample t-test.

Whole brain graph-derived metrics

An in-house Matlab® application was used to calculate the variance normalised (i.e., mean = 0; variance = 1 standard deviation) signal inside 152 specific regions of interest (ROI's) (Kim et al., 2023) for each of the subject's pre-processed resting state data. Pearson's correlation coefficient (r) was then calculated between the signal in each ROI and that of all other ROIs (ROI to ROI), in a pairwise manner, resulting in a 152 x 152 correlation matrix for each subject. Fisher z-transform was also calculated for each correlation matrix.

Network based statistics of whole brain graph

The Network-Based Statistics (NBS) Toolbox (Zalesky et al., 2010) was used to calculate differences in brain connectivity between drug and vehicle. First, a two-sample t-test was performed for every pairwise z-transformed Pearson's correlation coefficient comparing drug versus vehicle. Correlations that surpassed an initial threshold of $t > 3.1$ were subject to 5000 permutations using the false discovery rate (FDR) approach, which trades-off stringent control of false positives for the capacity to perform inference at the level of individual connections. The choice of threshold is arbitrary and has been levelled as a criticism of this approach (see NBS manual (Zalesky et al., 2010) however a previous work used $t = 3.1$ for a similar approach (Munoz-Moreno et al., 2020). Each test generated a 152 x 152 matrix representing the edges that show significant differences in magnitude between the groups. FDR-derived p-values <= 0.05 were considered statistically significant.

Circos (Krzywinski et al., 2009) was used to visualise the differences in brain connectivity between the drug and vehicle treated rats: one connectogram was created for each drug/vehicle comparison showing the edges that surpassed the initial t-test threshold.

Whole brain analysis of graph metrics

Graph theory metrics were calculated using MATLAB 2020a, and the Brain Connectivity Toolbox (Rubinov and Sporns, 2010). To minimise the influence of arbitrary threshold boundaries and spontaneous correlations, variance normalised adjacency matrices, derived from the full in-house atlas (152 nodes) (Kim et al., 2023), were subject to proportional thresholding at a range of graph densities from 5 % to 50 % in 5 % increments, where each density represents the strongest connections as a percentage of all possible connections between regions. Thus, weighted undirected graphs of the strongest connections were created, and from these, overall functional connectivity, global efficiency and average clustering coefficient were calculated for each subject at each graph density.

Overall functional connectivity (van den Heuvel et al., 2017) was calculated as the mean absolute value of the Fisher transformed correlation coefficients, excluding zeros. Global efficiency was calculated as the average inverse shortest path length in the network, as calculated with Dijkstra's algorithm. The clustering coefficient was calculated as the average geometric mean of all triangles associated with each node (Onnela et al., 2005), and the average across all nodes was taken as the average clustering coefficient.

For each metric, the group mean values were integrated as a function of graph density, and the area under the curve (AUC) was calculated using trapezoidal numerical integration (Ginestet et al., 2011). The difference in AUC was tested with a non-parametric permutation test, whereby the group labels at each time point are interchanged 5000 times to generate a null distribution of possible differences in

AUC, against which the observed difference is compared. P-values are calculated as the count where the absolute value of the random distribution is equal to or greater to the absolute value of the observed difference, divided by the number of permutations.

Network-constrained analysis of graph metrics

A priori network nodes were identified for the default mode network (DMN), the salience network (SN), and the basal ganglia (BG) network (Figure 4A), based on previous clinical literature that suggest changes in connectivity following administration of cannabis (Wall et al., 2019; Volkow et al., 1996). The ROIs for DMN were (bilateral): dorsal and ventral hippocampus, and cortices (prefrontal, auditory, cingulate, parietal, retrosplenial and visual) (Lu et al., 2012). The ROIs for salience network were (bilateral) insula and cingulate, chosen according to the recommendation by (Tsai et al., 2020). The ROIs for basal ganglia network were (bilateral) striatum, motor cortex and cingulate cortex (Sierakowiak et al., 2015). Variance normalised adjacency matrices from the functional atlas (MacNicol, 2021) (44 nodes, Supplementary Figure 1A) were not subject to thresholding due to the greatly reduced number of edges compared to the whole brain matrices. Instead, the previously described global metrics were calculated for each of these networks without thresholding. Since only one value was calculated per metric (compared to one for each graph density), functional connectivity, global efficiency and clustering coefficient were compared between drug and vehicle by two-way repeated measures ANOVA using GraphPad Prism v9.0.1.

Tissue sampling

After scanning, the rats were additionally deeply anaesthetised with 5% isoflurane in oxygen/air mix (1:9). They were decapitated. From animals treated with THC or CBD, a blood sample (0.6 ml) was collected into EDTA collection tube (Sarstedt Multivette 600 K3E) and spun at 10,000 rpm for 2 minutes. Samples were centrifuged within 5 min of collection. Aliquot of plasma (100 μl) was pipetted into clean labelled vials (Treff Microtube LockFit 1.5mL Natural DNAse/RNAse free (Anachem 95016313)) and stored frozen (-80ºC) until transfer for bioanalysis. Samples were frozen immediately on dry ice and remained on dry ice until transfer to -80 ºC freezer. Plasma for one vehicle animal for each vehicle was also collected in the same way (as much as could be obtained) for use as a blank. Brain was extracted of all rats treated with THC or CBD, weighed, divided into two hemispheres, and weighed. The left brain (LBRN) hemisphere was placed into a labelled vial (Safe lock Eppendorf 2.0 ml green (e.g. T2796, Sigma Aldrich)) and immediately frozen on dry ice (-80ºC) until transfer for bioanalysis. Whole brain from one vehicle animal for each vehicle was also collected and snap frozen in isopentane on dry ice for use as a blank.

Supplementary Materials

Supplementary Table 1: Total plasma and brain concentration of THC and CBD and metabolites at approximately 4 hours post-dose. – not analysed and BLQ < lower limit of quantification (<LLOQ), as shown below.

Dose, compound administered and route of administration	Tissue	Analyte measured (ng/mL plasma; ng/g brain) [median (interquartile range)]						
		CBD	7-COOH CBD	6-OH CBD	7-OH CBD	THC	11-OH THC	11-COOH THC
CBD, 150 mg/kg, i.p	plasma	1530 (1408)	358 (572)	90.5 (76.4)	104 (91.4)	–	–	–
	brain	2140 (4083)	20.9 (11.2)	68.4 (71.4)	105 (61.7)	11.4 (21.7)	BLQ	BLQ
THC, 10 mg/kg, i.p	plasma	–	–	–	–	40.6 (35)	14.3 (17.6)	17.1 (15.6)
	brain	–	–	–	–	165 (113)	146 (102)	12 (9.83)
THC 10.8 mg/kg: CBD 10 mg/kg, i.p.	plasma	99.7 (113)	32.6 (36.1)	9.86 (12.5)	17.8 (12.2)	175 (207)	15 (10.8)	5.27 (3.23)
	brain	181 (180)	BLQ	10 (8.19)	BLQ	694 (695)	100 (73.1)	4.60 (3.03)
LLOQ (ng/mL)	plasma	4	4	0.5	0.5	0.25	0.5	0.5
LLOQ (ng/g)	brain	4	4	0.5	20	0.25	0.5	0.5

Supplementary Figures

Figure S1: ROIs

A

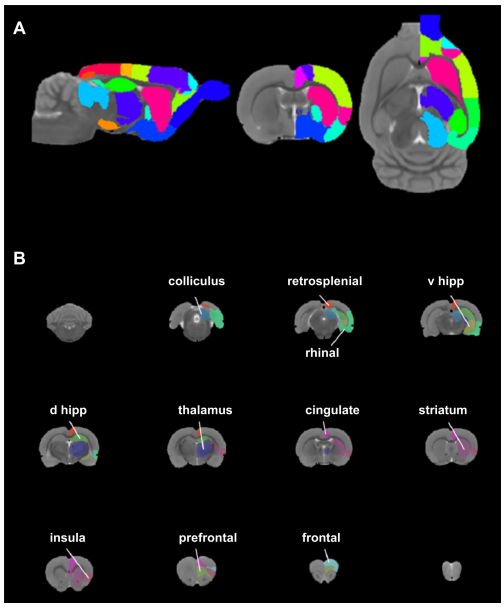

B

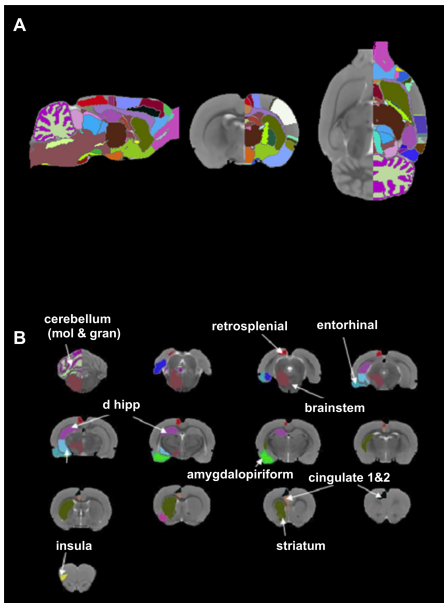

Atlas delineations of regions of interests (ROIs).

Figure S1A

The 44 bilateral ROIs used for CBF analysis (showing one side only), overlaid on a template image to illustrate the ROIs' spatial distribution in A) sagittal, coronal, and axial planes and B) slices of the coronal plane.

Figure S1B

The 152 bilateral ROIs, which were used for BOLD analyses (showing one side only), overlaid on a template image to illustrate the ROIs' spatial distribution in A) sagittal, coronal, and axial planes and B) slices of the coronal plane.

Abbreviations: mol = molecular; gran = granular; hipp = hippocampus.

Figure S2: extra seeds

A

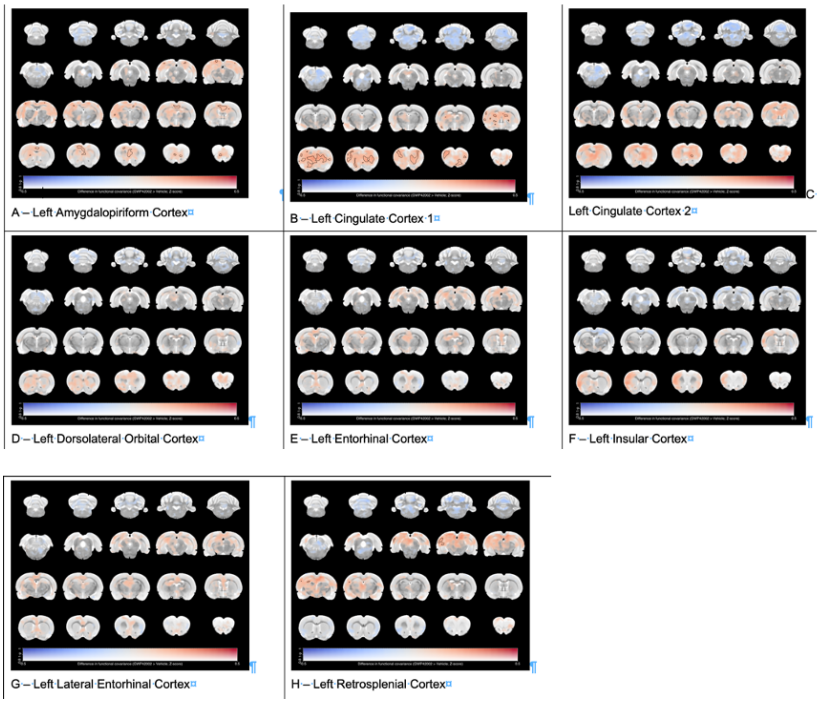

B

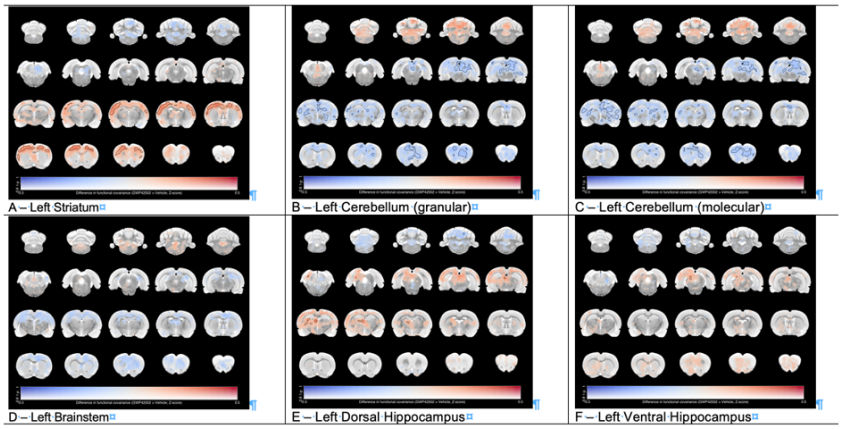

C

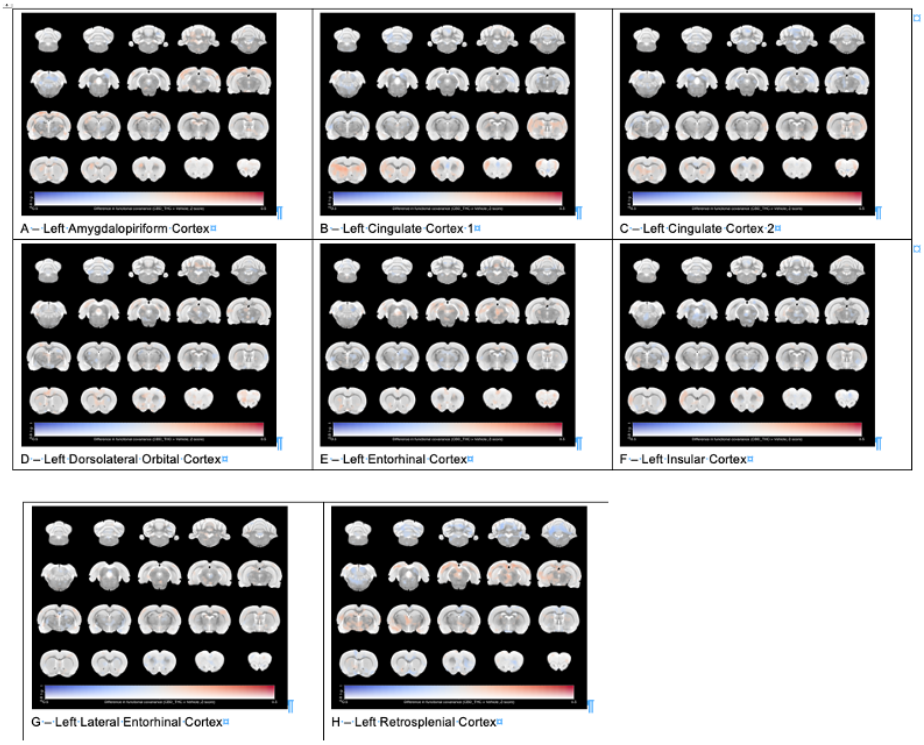
A – Left Amygdalopiriform Cortex
B – Left Cingulate Cortex 1
C – Left Cingulate Cortex 2
D – Left Dorsolateral Orbital Cortex
E – Left Entorhinal Cortex
F – Left Insular Cortex
G – Left Lateral Entorhinal Cortex
H – Left Retrosplenial Cortex

D

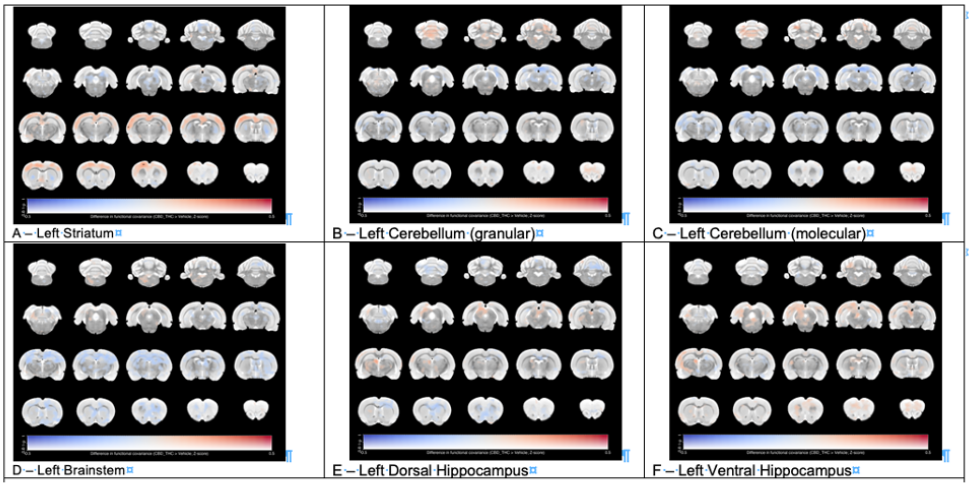
A – Left Striatum
B – Left Cerebellum (granular)
C – Left Cerebellum (molecular)
D – Left Brainstem
E – Left Dorsal Hippocampus
F – Left Ventral Hippocampus

E

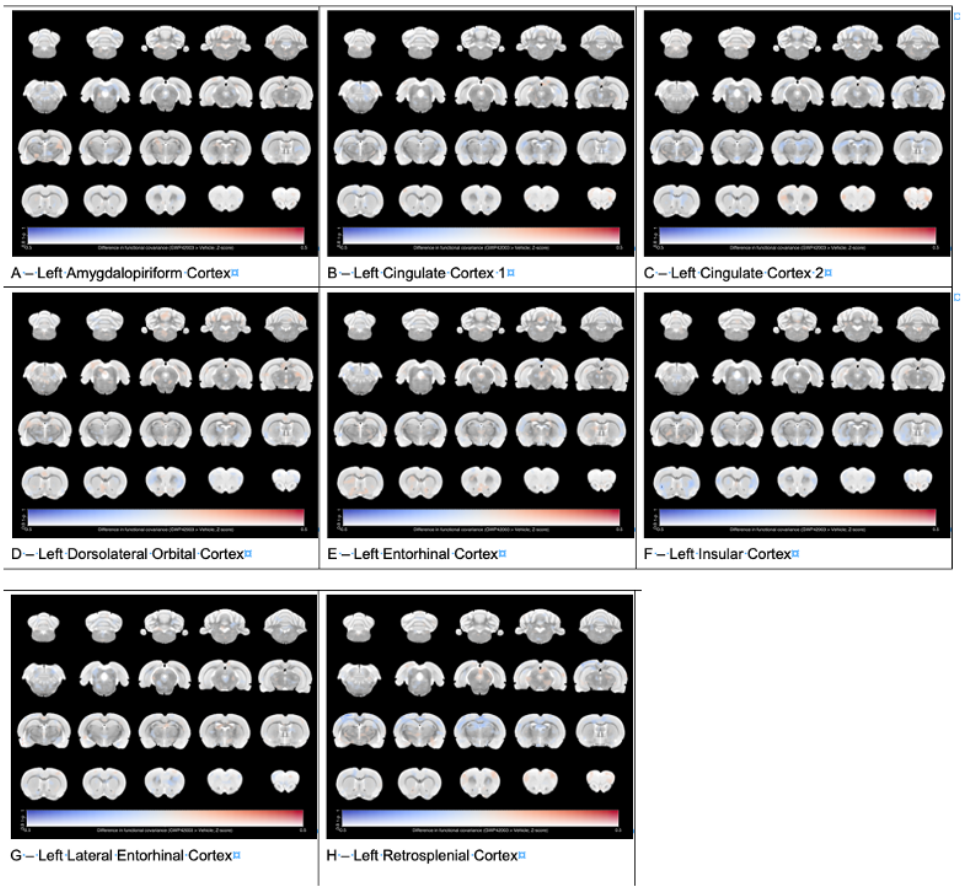

F

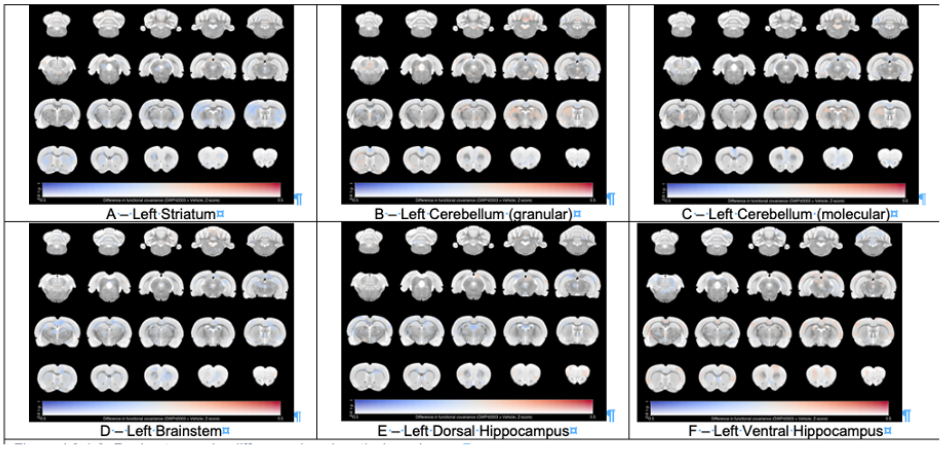

Seed correlations

A, B: THC cortical, subcortical

C, D: THC:CBD cortical, subcortical

E, F: CBD cortical, subcortical

Figure S3 – FC and CBF correlations

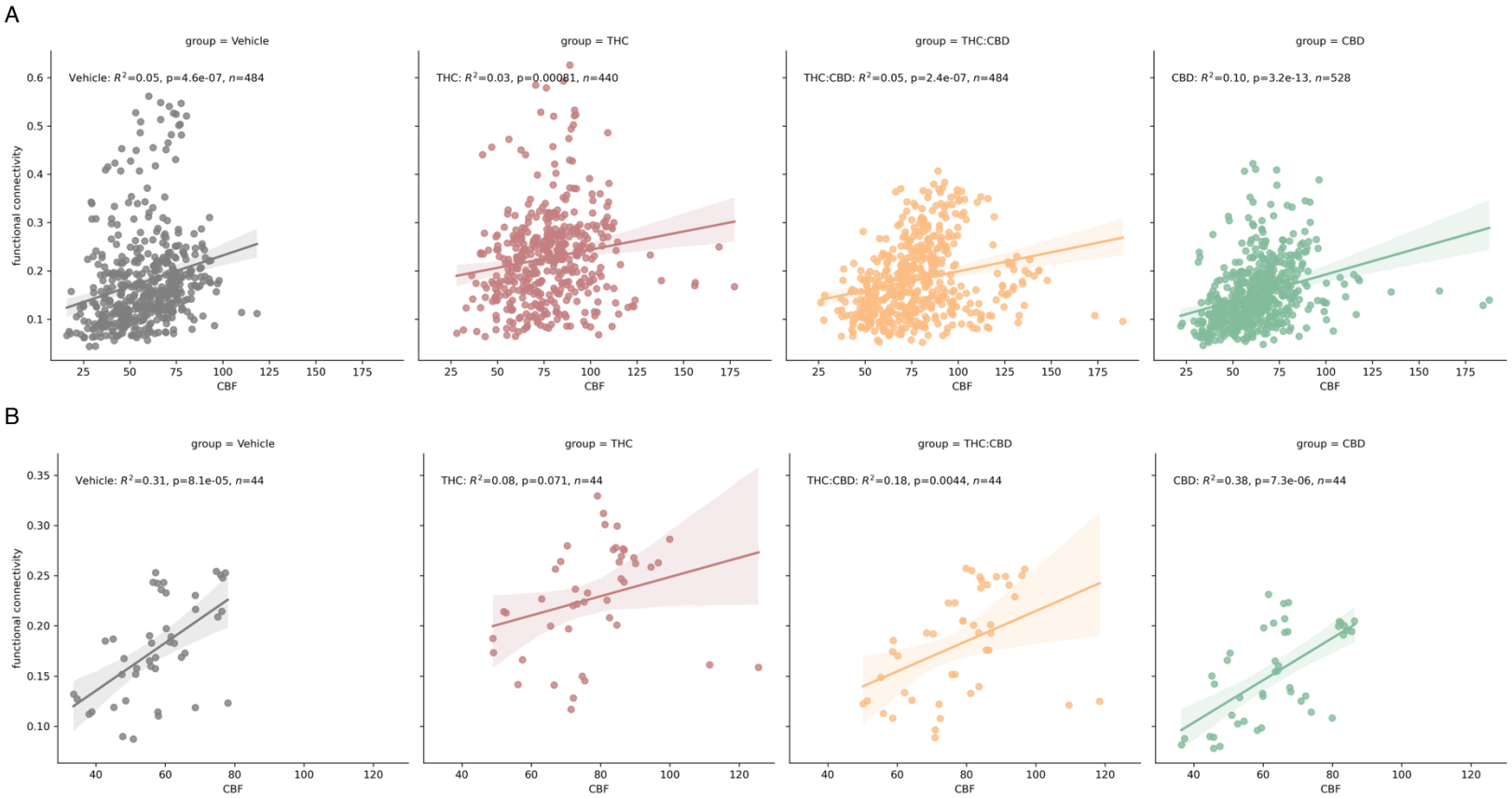

Figure S3: Scatterplots of the relationship between mean regional Cerebral Blood Flow (CBF) and mean functional connectivity strength.

Each point is an ROI (A, all subjects, B, averaged across all subjects) with a line of best fit defined by ordinary least squares model and a 95% confidence interval (ribbon) for each group. Each subplot represents the scores from a different drug group ccording to colour coding.

References

Andersson JL, Skare S and Ashburner J (2003) How to correct susceptibility distortions in spin-echo echo-planar images: application to diffusion tensor imaging. *Neuroimage* 20(2): 870-888.

Batalla A, Crippa JA, Busatto GF, et al. (2014) Neuroimaging studies of acute effects of THC and CBD in humans and animals: a systematic review. *Curr Pharm Des* 20(13): 2168-2185.

Ginestet CE, Nichols TE, Bullmore ET, et al. (2011) Brain network analysis: separating cost from topology using cost-integration. *PLoS One* 6(7): e21570.

Hallquist MN, Hwang K and Luna B (2013) The nuisance of nuisance regression: spectral misspecification in a common approach to resting-state fMRI preprocessing reintroduces noise and obscures functional connectivity. *Neuroimage* 82: 208-225.

Kim E, Figueiredo IC, Simmons C, et al. (2023) Mapping acute neuroinflammation in vivo with diffusion-MRI in rats given a systemic lipopolysaccharide challenge. *Brain Behav Immun*. Epub ahead of print 20230721. DOI: 10.1016/j.bbi.2023.07.010.

Klein A, Andersson J, Ardekani BA, et al. (2009) Evaluation of 14 nonlinear deformation algorithms applied to human brain MRI registration. *Neuroimage* 46(3): 786-802.

Krzywinski M, Schein J, Birol I, et al. (2009) Circos: an information aesthetic for comparative genomics. *Genome Res* 19(9): 1639-1645.

Liang Z, Li T, King J, et al. (2013) Mapping thalamocortical networks in rat brain using resting-state functional connectivity. *Neuroimage* 83: 237-244.

Lu H, Zou Q, Gu H, et al. (2012) Rat brains also have a default mode network. *Proc Natl Acad Sci U S A* 109(10): 3979-3984.

MacNicol E (2021) *Longitudinal Characterisation of Healthy Ageing in Rats using Multimodal Magnetic Resonance Imaging*. PhD, King's College London.

Munoz-Moreno E, Tudela R, Lopez-Gil X, et al. (2020) Brain connectivity during Alzheimer's disease progression and its cognitive impact in a transgenic rat model. *Netw Neurosci* 4(2): 397-415.

Oguz I, Zhang H, Rumple A, et al. (2014) RATS: Rapid Automatic Tissue Segmentation in rodent brain MRI. *J Neurosci Methods* 221: 175-182.

Onnela JP, Saramaki J, Kertesz J, et al. (2005) Intensity and coherence of motifs in weighted complex networks. *Phys Rev E Stat Nonlin Soft Matter Phys* 71(6 Pt 2): 065103.

Rubinov M and Sporns O (2010) Complex network measures of brain connectivity: uses and interpretations. *Neuroimage* 52(3): 1059-1069.

Sadagopan S, Temiz-Karayol NZ and Voss HU (2015) High-field functional magnetic resonance imaging of vocalization processing in marmosets. *Sci Rep* 5: 10950.

Sierakowiak A, Monnot C, Aski SN, et al. (2015) Default mode network, motor network, dorsal and ventral basal ganglia networks in the rat brain: comparison to human networks using resting state-fMRI. *PLoS One* 10(3): e0120345.

Spisak T, Spisak Z, Zunhammer M, et al. (2019) Probabilistic TFCE: A generalized combination of cluster size and voxel intensity to increase statistical power. *Neuroimage* 185: 12-26.

Tsai PJ, Keeley RJ, Carmack SA, et al. (2020) Converging Structural and Functional Evidence for a Rat Salience Network. *Biol Psychiatry* 88(11): 867-878.

Tustison NJ, Avants BB, Cook PA, et al. (2010) N4ITK: improved N3 bias correction. *IEEE Trans Med Imaging* 29(6): 1310-1320.

van den Heuvel MP, de Lange SC, Zalesky A, et al. (2017) Proportional thresholding in resting-state fMRI functional connectivity networks and consequences for patient-control connectome studies: Issues and recommendations. *Neuroimage* 152: 437-449.

van Lieshout LLF, Vandenbroucke ARE, Muller NCJ, et al. (2018) Induction and Relief of Curiosity Elicit Parietal and Frontal Activity. *J Neurosci* 38(10): 2579-2588.

Volkow ND, Gillespie H, Mullani N, et al. (1996) Brain glucose metabolism in chronic marijuana users at baseline and during marijuana intoxication. *Psychiatry Res* 67(1): 29-38.

Wall MB, Pope R, Freeman TP, et al. (2019) Dissociable effects of cannabis with and without cannabidiol on the human brain's resting-state functional connectivity. *J Psychopharmacol* 33(7): 822-830.
Wood TC (2016) QUIT: QUantitative Imaging Tools. *The Journal of Open Source Software* 3.
Zalesky A, Fornito A and Bullmore ET (2010) Network-based statistic: identifying differences in brain networks. *Neuroimage* 53(4): 1197-1207.